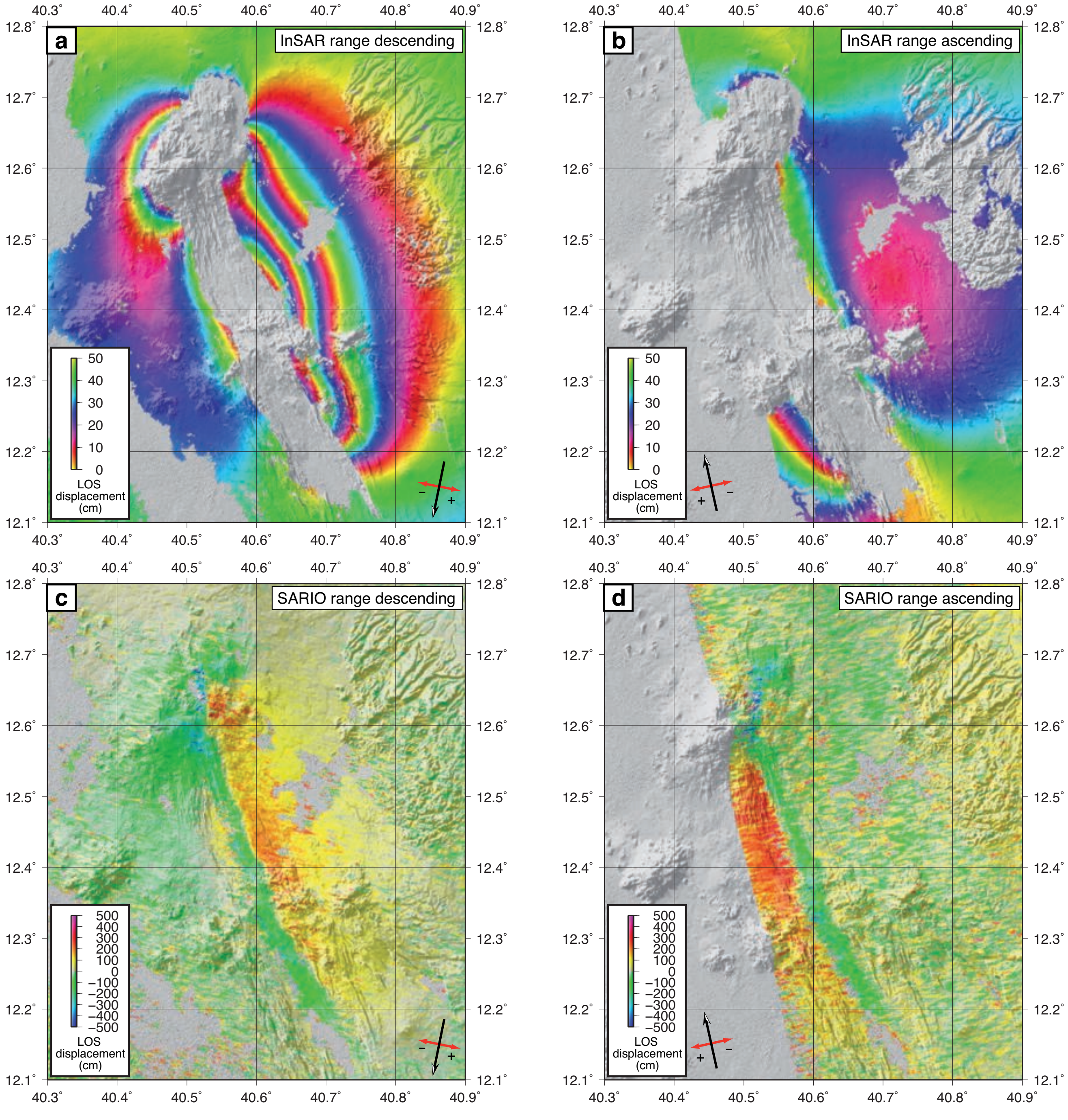

Figure S-1. Deformation obtained by InSAR on descending (top left) and ascending (top right) orbits, and by SARIO along range on descending (bottom left) and ascending (bottom right) orbits. Motion towards the satellite gives a positive value (red arrow). Because the angle of incidence is nearly vertical ($\sim 70°$), measurements are mostly sensitive to the vertical component of deformation; the difference between ascending and descending measurements originates from a different sensitivity to horizontal components of displacement.

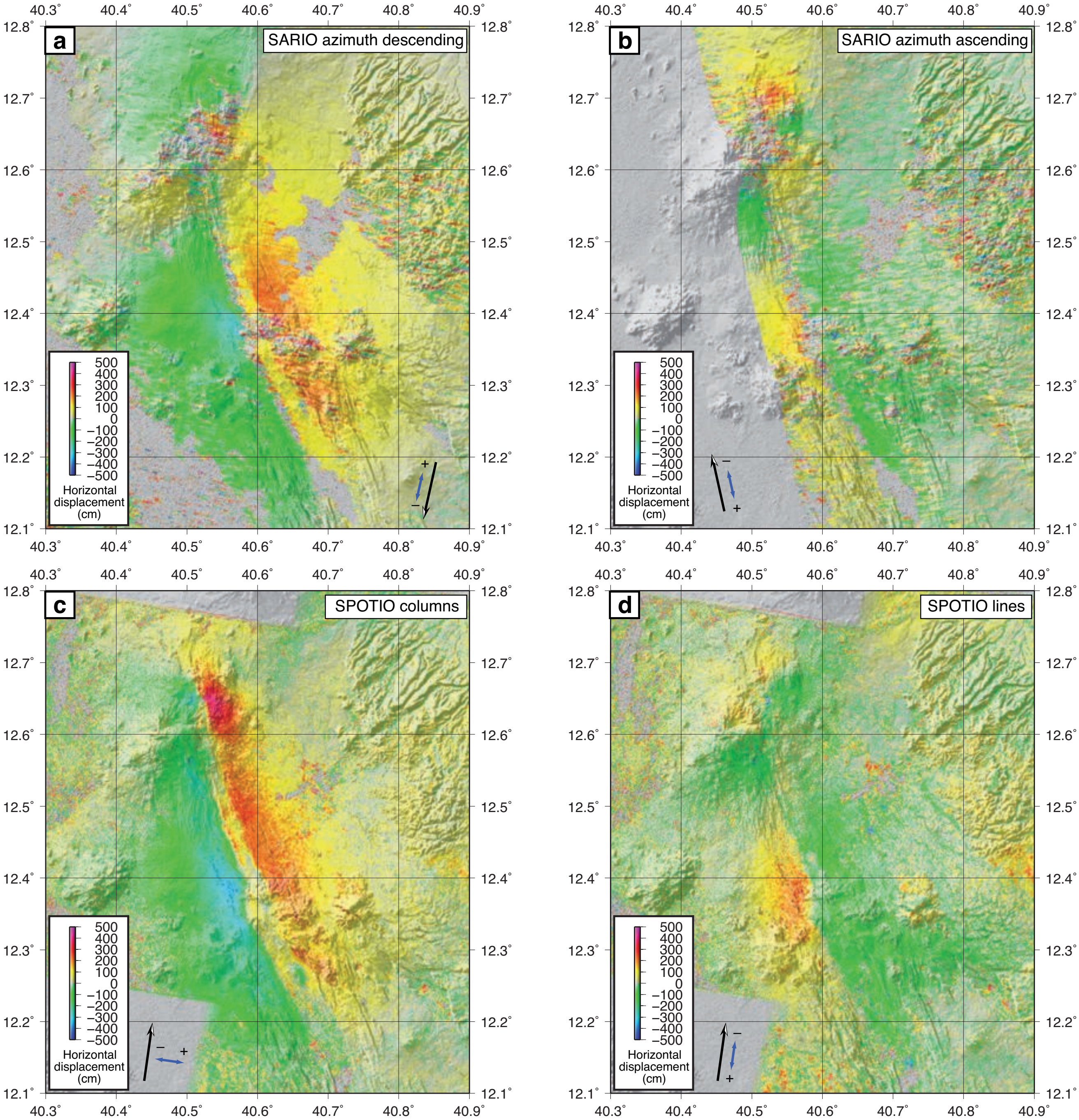

Figure S-2. Deformation obtained by SARIO along azimuth on descending (top left) and ascending (top right) orbits, and by SPOTIO along columns (bottom left) and rows (bottom right). These measurements are only sensitive to one particular direction of the horizontal component of deformation (blue arrow).

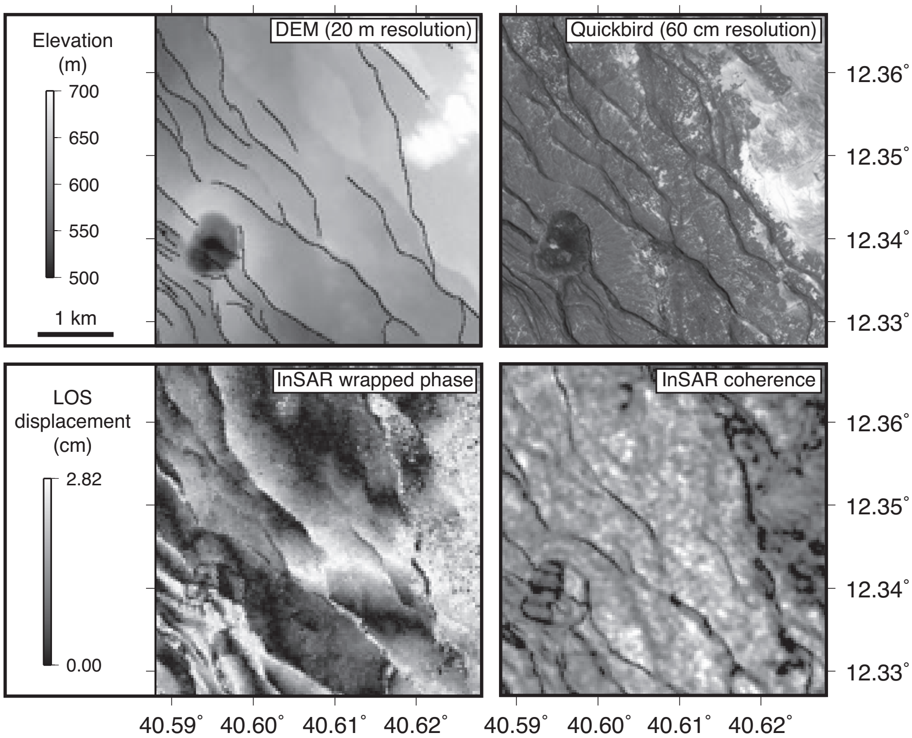

Figure S-3. Data set used for the mapping of the faults activated during the 2005 episode. The SPOT5 based DEM (top left) provides a first insight on the relative importance of the scarps associated with discontinuities in post-September 2005 InSAR images (bottom left). Mapping is further completed by comparison with high-resolution Quickbird imagery (top right) and InSAR correlation (bottom right), which is usually low along the surface trace of moving faults. The frame is approximately 4 km wide, and focussed on the caldera that outcrops within the axial basaltic graben floor, at the latitude of the Ado'Ale Volcanic Complex.

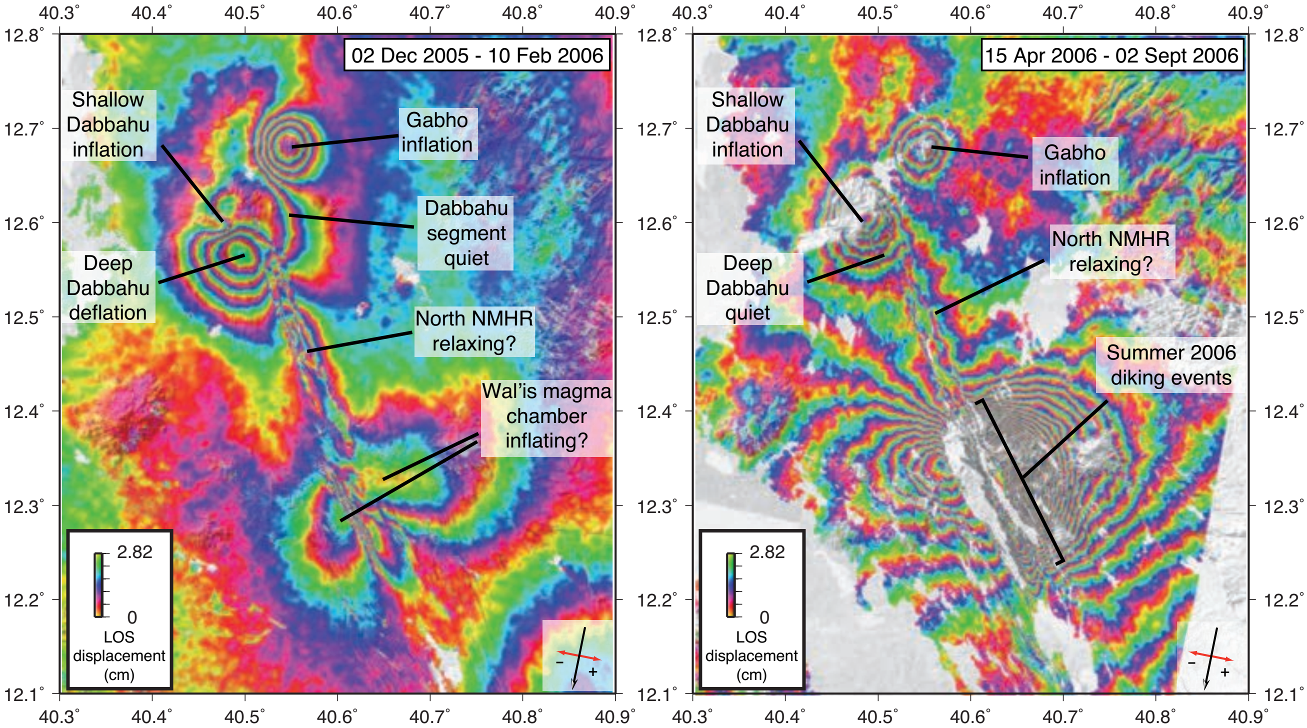

Figure S-4. Deformation measured by InSAR, in the time span between + 2 months and + 4 months (left), and between + 6 months and + 11 months (right) after the September 2005 rifting event. The second interferogram captures the dike intrusions of June 17 and July 25 2006 [*Keir et al.*, 2008; *Hamling et al.*, 2008]. Both interferograms were obtained from descending track SAR images (looking from the ESE), but the look angle of the latest image is less vertical, thus including a larger component of horizontal deformation in the measurement. Each color cycle corresponds to a displacement projected onto the line of sight of 2.82 cm (one color cycle in Figure S-1 is equivalent to 17 cycles in Figure S-4). In the few months following the September 2005 rifting event, subsidence in the Dabbahu area was sustained, and can be attributed to deflation of the deep (∼ 9 km depth) Dabbahu magmatic chamber. It was then replaced by the inflation of a much shallower (∼ 3 km depth) magmatic chamber, slightly offset to the North, that inflated a decreasing rate at least until 2009. On the other hand, the Gabho magmatic chamber re-inflated at a decreasing rate immediately after the rifting event until 2007. The dikes that were emplaced during the summer 2006 within the Northern Manda Hararo Rift were not fed from the Dabbahu and Gabho magmatic chambers. The fringes occurring off-axis at 12.30°N are caused by the inflation of the deep Wal'is magma chamber.

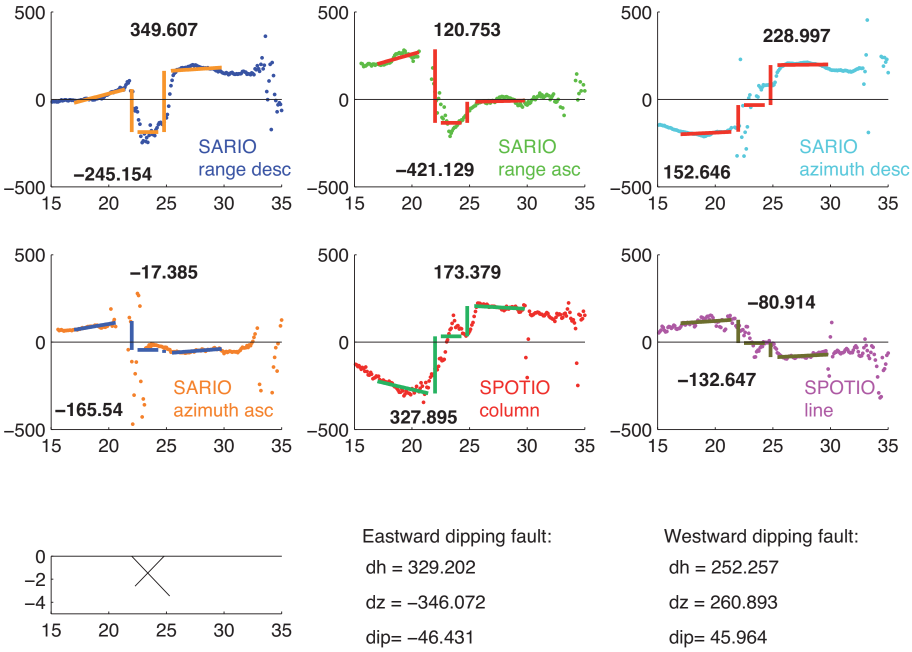

Figure S-5. Example of the process of estimation of the offset across rift border faults, using the six components of surface displacements available in the near field. For each component, the observed profile is fit by a piecewise linear curve made of three segments, with the central curve being forced to remain horizontal. The two discontinuities of the fitted curve at the location of the border fault provide a stable measurement of the projected offset (bold figures at the top and bottom of each curve). The result is then used to estimate the vertical and horizontal component of deformation, by performing a simple least-squares inversion.

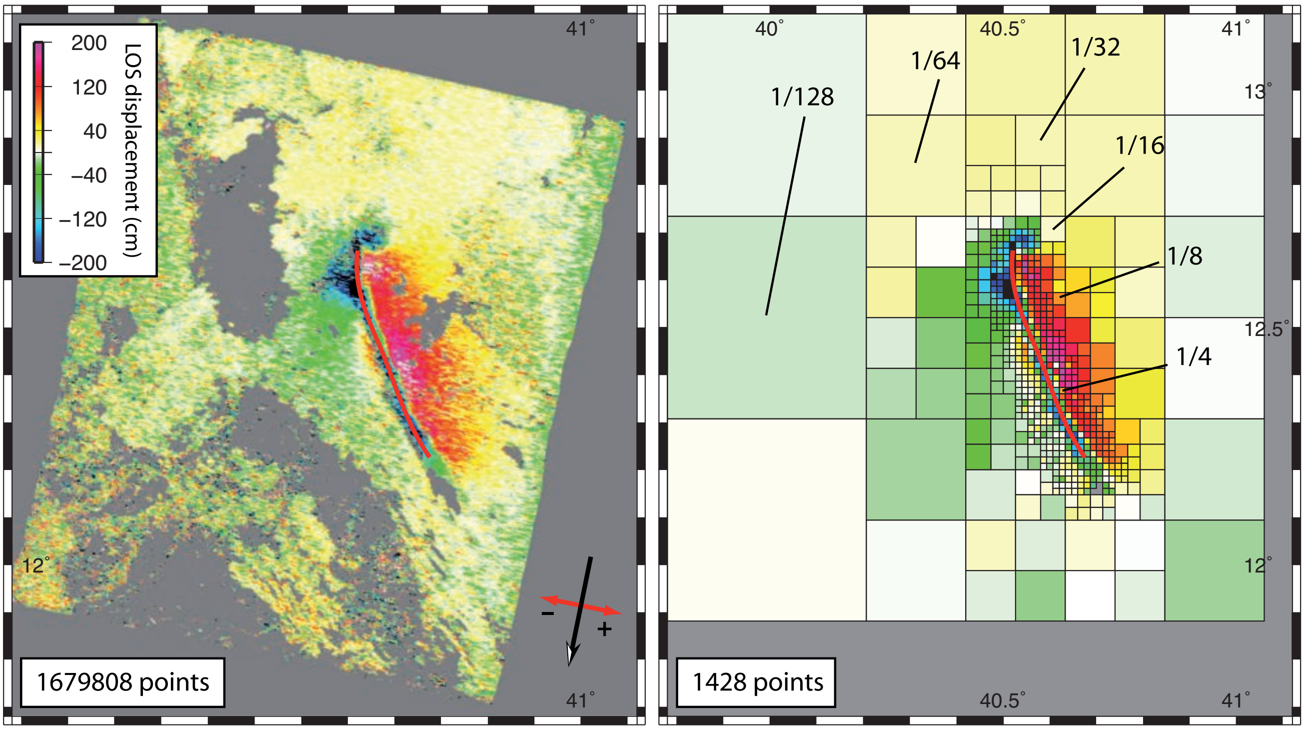

Figure S-6. SARIO range descending offsets, prior (left) and after (right) downsampling. Starting from a very coarse resampling, the data set is stored into a quad-tree structure. Each node can then be subdivided into four smaller nodes, corresponding to the four quadrants of the former node, thus increasing the sampling density a factor of 4. The distance between the center of each square (a node of the quadtree) and the dike (red line) is used as a criterion to decide whether further subdivision of the node is required. Here, the sampling rate is increased as the inverse of the cubic power of the distance from the rift (a proxy of the strain). This process is applied to each data set independently, but with the same distance criterion. This leads to a uniform sampling density of each data set within each distance range, and thus to a globally equilibrated weight of each measured component of deformation.

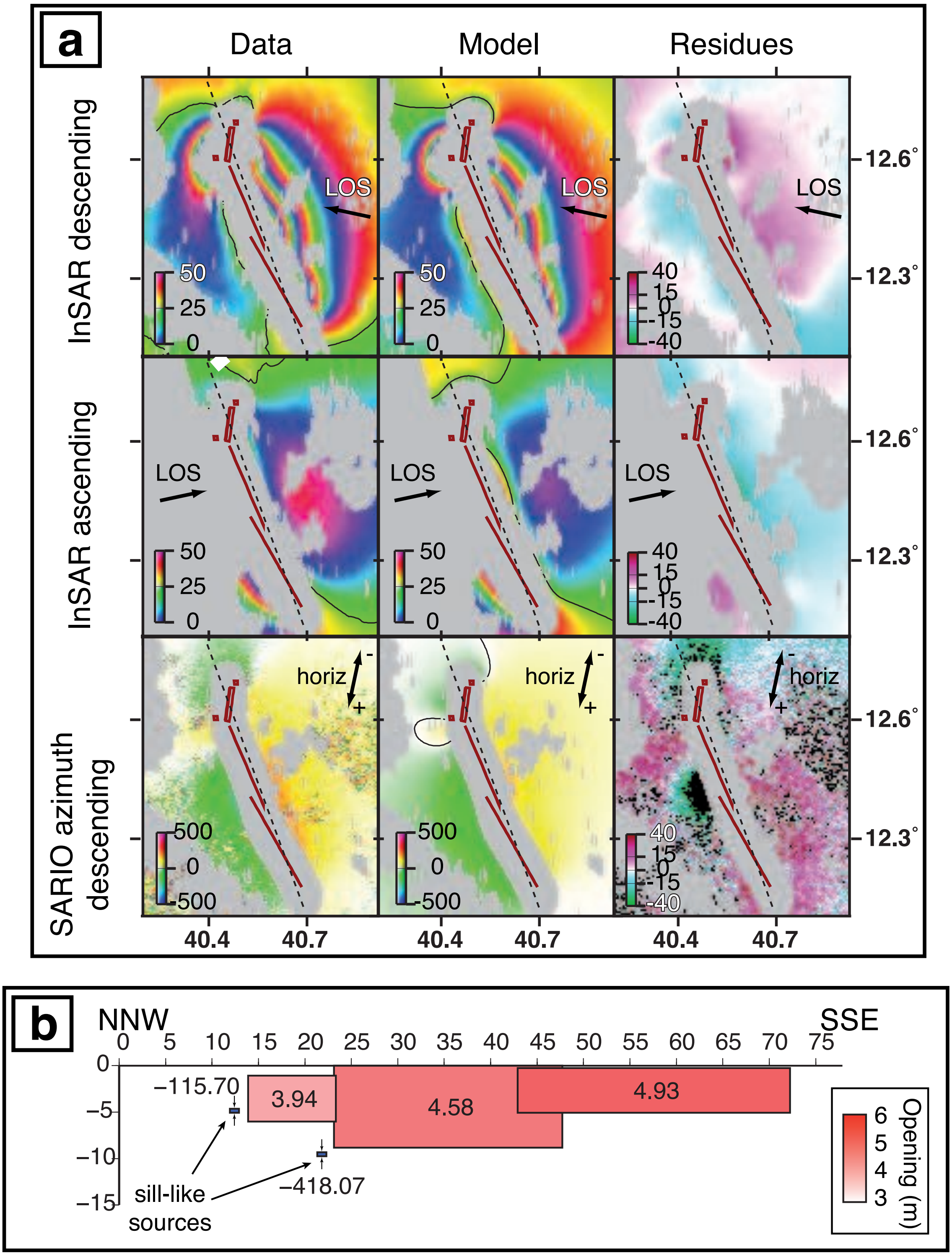

Figure S-7. a) Comparison of observed (left), modeled (center) and residual (right) far-field displacements obtained for the inversion of the geometric parameters of the dike and magmatic chambers. b) Cross-sectional view of the opening distribution deduced from this inversion, projected onto an along-axis direction. Dashed lines in a) show the approximate location of the profile.

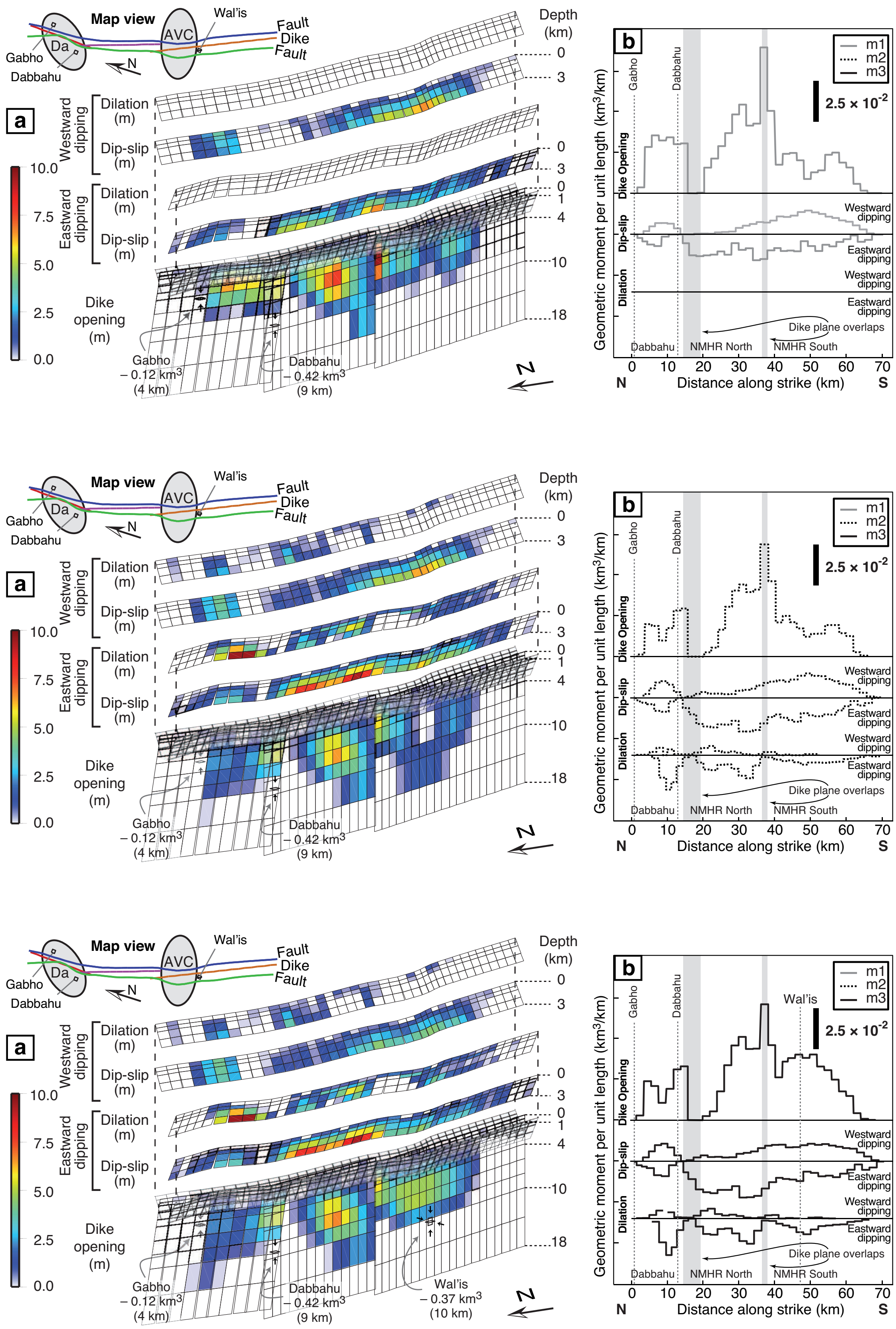

Figure S-8. Comparison of solutions m1 (top), m2 (middle) and m3 (bottom).

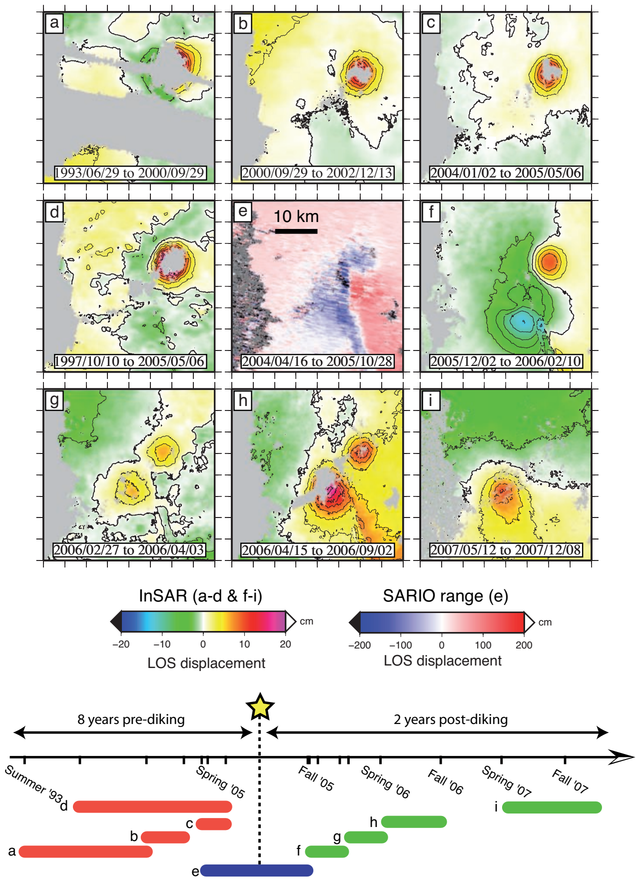

Figure S-9. Displacement of the ground surface, projected onto the line of sight of the satellite, determined by InSAR (a-d & f-i) and SARIO range (e). Each frame corresponds to a time span sketched by the horizontal color bars at the bottom (time scale is different before and after the September rifting 2005 event). Measurements are mostly sensitive to the vertical component of deformation, and provide a straightforward assessment of the amount of contraction or dilation at depth that is caused by variations of pressure inside the magma reservoirs. Color scales are different for InSAR and SARIO measurements (red for inflation, blue for deflation). A small rifting event occurred at Gabho between 1993 and 1997 (a). Prior to the September rifting 2005 event, accelerating uplift is detected above Gabho volcano (b-d). During the September 2005 event, the deep Dabbahu ($\sim$ 9 km depth) and Gabho ($\sim$ 4 km depth) both deflate, possibly as a result of the drainage of the magma out of the magmatic chamber, into the dike (e). Inflation of the Gabho magma chamber resumed after the main rifting event, until late 2006 (f-h). Until 3 ± 1 months after the September 2005 rifting event, the deep Dabbahu magma chamber continued to deflate, possibly as a result of a sustained connection with the dike (f). Approximately at the same time as deflation stopped at deep Dabbahu magma chamber, a shallow magma chamber ($\sim$ 4 km depth), slightly offset to the NW by $\sim$ 5 km, starts to inflate (f-i).

Table 1. Time intervals covered by the geodetic data presented in this study.

Data	Image location/type	Image A	Image B	Temporal baseline (days)	Perpendicular baseline (m)	Post-diking time spanned (days)
InSAR/SARIO	descending	16/04/04	28/10/05	560	30	33
	ascending	28/07/04	26/10/05	455	385	31
SPOTIO	SE	21/02/05	25/01/06	338	-	122
	NE	21/02/05	25/01/06	338	-	122
	NW	19/12/04	13/01/06	390	-	110

Table 2. Geometric features of the various components of displacement measured by InSAR, SARIO and SPOTIO, and associated errors.

Data set		InSAR descending	InSAR ascending	SARIO range descending	SARIO range ascending	SARIO azimuth descending	SARIO azimuth ascending	SPOTIO row	SPOTIO column
Typical measurement error		1 cm	1 cm	50 cm	50 cm	30 cm	30 cm	20-100* cm	20-100* cm
Azimuth (clockwise, with respect to North)		102.5°	257.5°	102.5°	257.5°	192.5°	347.5°	188.0°	278.0°
Incidence angle (with respect to vertical)		22°	18°	22°	18°	90°	90°	85-90°	85-90°
Projection vector	E-W	0.359	-0.270	0.359	-0.270	0.216	0.216	0.988	-0.153
	N-S	-0.079	-0.059	-0.079	-0.059	0.976	-0.976	-0.153	-0.988
	U-D	0.932	0.961	0.932	0.961	0.000	0.000	0.000	0.000

*: depending on the spatial wavelength of the signal (see text for discussion)

Table 3. Data set used for the inversion.

Data set	InSAR descending	InSAR ascending	SARIO range descending	SARIO range ascending	SARIO azimuth descending	SARIO azimuth ascending	SPOTIO row SE	SPOTIO row NE	SPOTIO row NW	SPOTIO column SE	SPOTIO column NE	SPOTIO column NW	Total
Original number of points	1347418	2713781	1595333	678321	1489605	654413	102627	144153	143561	102627	144153	143561	9259553
Downsampled number of points	1420	1500	585	556	585	555	138	126	240	138	126	240	6209
Weight (%)	22.87	24.16	9.42	8.95	9.42	8.94	2.22	2.03	3.87	2.22	2.03	3.87	100.00